Effects of vent overpressure on buoyant eruption columns: Implications for plume stability

Darcy E. Ogden [a],*, Gary A. Glatzmaier [a], Kenneth H. Wohletz [b]

[a] *Earth & Planetary Sciences Department, University of California at Santa Cruz, 1156 High Street, Santa Cruz, CA 95064, USA*
[b] *Los Alamos National Laboratory, EES11 MS F665, Los Alamos, NM 87545, USA*

Abstract

Volcanic plumes resulting from explosive volcanic eruptions present a variety of hazards depending on their behavior. Buoyant plumes heat and entrain enough of the surrounding air to rise high into the atmosphere, disrupting air traffic and causing regional ash fall. Alternatively, collapsed plumes produce dangerous fast-moving lateral flows of hot ash and gas. The transition between these behaviors and the nature of each hazard is dependent on the fluid dynamics of the volcanic plume, which is largely determined by the conditions at the vent. Most treatments of volcanic plumes for hazard assessment assume that the eruptive fluid exits the vent at pressures equal to atmospheric pressure or that pressure equalizes quickly with little effect on the flow. Here we show that vent pressures greater than atmospheric lead to rapid expansion of the plume and the development of standing shock waves that change the behavior of the entire eruption column. We simulate two volcanic plumes with the same heat flow ($J\ s^{-1}$) at the vent; one exits the vent at atmospheric pressure (pressure-balanced) and the other at four times atmospheric pressure (overpressured). The two simulated plumes have the same radius after the initial rapid decompression of the overpressured case. These plumes show drastically different behavior due to the presence of standing shock waves in the overpressured case despite having the same heat flow at the vent and the same area available for entrainment of ambient air. Both simulated plumes exhibit buoyant rise but the overpressured plume collapses with a regular periodicity. These simulations suggest that the dynamics of a steady-state overpressured vent may result in plumes that oscillate between buoyant rise and collapse, providing a mechanism for the deposition of intraplinian pyroclastic flows.
© 2008 Elsevier B.V. All rights reserved.

Keywords: eruption; overpressure; plume; simulation; transitional column

1. Introduction

Analysis and modeling of volcanic eruption columns began over 30 yr ago (e.g. Walker et al., 1971; Wilson et al., 1978) and has evolved to a point where quantitative predictions can be made concerning their impact on the Earth's atmosphere and surface (e.g. Carey and Sparks, 1986; Woods, 1988; Aloisi et al., 2002). Mathematical modeling of volcanic eruption columns has been primarily one dimensional (1D), including the recognition that eruption columns can collapse like a fountain to form pyroclastic flows. In such an analysis collapsing eruption column behavior happens at the expense of buoyant plume rise when there is insufficient entrainment and heating of air to make the column buoyant (Sparks and Wilson, 1976). Two and three-dimensional computational simulations have provided more detail but have generally supported the results of 1D analysis (e.g. Valentine and Wohletz, 1989; Papale et al., 1998; Suzuki et al., 2005; Neri et al., 2007).

Observations and analysis generally characterize eruption column structure as consisting of two major parts: a jet or gas-thrust region and a buoyant or plume region. The gas-thrust region at the base of the column consists of an eruptive mixture that is heavier than the surrounding air but moves upward with momentum derived from the expanding volcanic gases. Above the gas-thrust region, where the momentum of the eruptive mixture has decreased and the heating and expansion of entrained air makes the plume lighter than the surrounding

atmosphere, the upward motion in the plume region is controlled by buoyancy. The height of an eruption column is typically dominated by the plume region, which supports the classical theory of buoyant plumes (Morton et al., 1956). Such analysis shows a proportionality of the plume height with the quarter-root of the vent heat flow (Wilson et al., 1978). From that height, atmospheric dispersion of ash and pumice can be addressed by adaptations of classical Gaussian plume models or stochastic particle tracking methods (e.g. Carey and Sparks, 1986; Macedonio et al., 1990; Searcy et al., 1998; Ishimine, 2006). Detailed predictions are made for an eruption's impact on the surrounding areas with knowledge of fallout dynamics of ash and pumice as a function of their size distributions and densities (e.g. Macedonio et al., 1990). Inversion of historical ash deposit thickness and maximum clast-size data allows reconstruction of a volcanic eruption column and its mass eruption rate (e.g. Carey and Sparks, 1986; Hurst and Turner, 1999; Connor et al., 2001; Koyaguchi and Ohno, 2001a,b; Bonadonna et al., 2005). Additionally, studies have addressed the complicated effects of continual fragmentation of the magma throughout the conduit, vent and gas-thrust region, resulting in a continual evolution of clast-size and gas fraction of the eruptive fluid (Kaminski and Jaupart, 1998).

These existing 1D volcanic plume models assume either a top-hat shaped or Gaussian velocity distribution in radius throughout both regions of the eruption column with the peak vertical velocity occurring on the plume centerline (Sparks et al., 1997). This is an appropriate assumption for a jet exiting the vent at atmospheric pressure. 1D analysis and laboratory experiments (Kieffer, 1981; Kieffer and Sturtevant, 1984; Woods and Bower, 1995) have shown that explosive volcanic eruptions can produce a supersonic jet that may produce dramatic pressure gradients within the gas-thrust region. Furthermore, a recent numerical simulation study by Ogden et al. (2008) demonstrates how the standing shock waves produced in an overpressured volcanic jet can cause the development of an annular velocity profile with a slowly-moving core and rapidly moving outer annulus (Fig. 1a). Ogden et al. suggest that this velocity profile may result in entrainment rates that are different than those expected from a pressure-balanced plume, but they were unable to test this theory since their model did not include gravity or a stratified atmosphere.

Previous studies show that simple parameterized entrainment rates based on average vertical velocity profiles are not sufficient to capture the complicated dynamics of an eruption column. For example, Kaminski et al. (2005) show that jets that are denser than their surroundings have significantly reduced entrainment rates. Carazzo et al. (2006) detail some of the effects of scaling and velocity on entrainment rates of jets and buoyant plumes. Suzuki et al. (2005) quantify entrainment rates using a 3D simulation of a pressure-balanced volcanic plume. They demonstrate that entrainment at the base of the plume mainly takes place in the outer shear causing less entrainment than in the upper region of the plume where large scale instabilities dominate the dynamics. Their simulations also demonstrate the importance of including the third dimension in quantifying entrainment phenomena.
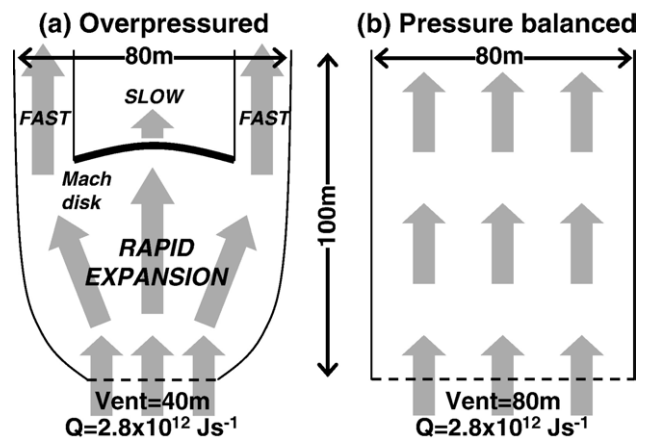

Fig. 1. Schematic overpressured (a) and pressure-balanced (b) jets of this study. Vents with sonic vertical velocity and fluid pressure greater than atmospheric result in a rapid expansion and acceleration of the fluid and the formation of a standing Mach disk that drastically reduces the vertical velocities in the core of the jet (a). Vents with sonic velocities and fluid pressure equal to atmospheric retain the velocity profile of the vent and have negligible change in plume radius at the base of the plume (b). The plume radius of an overpressured jet after expansion is roughly equal to the vent radius of a pressure-balanced jet with the same convective heat and mass flows at the vent (Section 2). We simulate an overpressured jet (a) with a vent radius of 20 m (40 m diameter) and a vent pressure of four times atmospheric and a pressured balanced jet (b) with a vent radius of 40 m (80 m diameter).

Here we modify the simulations of Ogden et al. (2008) to include gravity and a stratified atmosphere and perform a first-order test of the effect of vent overpressure on volcanic plume dynamics. We simulate two high-resolution plumes, one with atmospheric pressure at the vent and the other with a vent pressure four times greater than atmospheric. These plumes have the same heat flow (2.8×10^{12} J s^{-1}) and mass flow (3.5×10^{6} kg s^{-1}) at the vent and, after expansion of the overpressured jet, they have the same plume radius (Fig. 1). We show that the annular velocity profile in the overpressured jet persists throughout the gas-thrust region, leading to dramatically different flow dynamics than those predicted by analyses of pressure-balanced vents. Furthermore, we demonstrate that vent overpressure may cause a dynamic instability in an eruption column leading to a periodic collapse of the plume that may produce intraplinian pyroclastic flows (Wilson and Hildreth, 1997, 1998).

2. Methods

The computational domain for both simulations is a two-dimensional (2D) axisymmetric model of the Earth's atmosphere, 5 km in radius and 10 km in height. We include a downward gravitational acceleration (9.81 m s^{-2}) and density stratification of the ambient air in hydrostatic equilibrium based on a standard Earth atmosphere to simulate buoyancy forces in the plume (Appendix A). The top and side boundaries of the computational mesh are outflow boundaries. The bottom of the mesh is an impermeable free-slip boundary (the surface of the Earth) except for an inflow boundary at the center that represents the vent. The mesh consists of uniform grid cells

that are 2 m in both height and radius. Test simulations show that a courser mesh cannot capture the annular velocity profile above the Mach disk for the overpressured jet (Fig. 2). We have chosen to focus on the effects of the radial velocity profile and have neglected the complicating effects of gas exsolution and fragmentation that are included in many 1D models (e.g. Woods and Bower, 1995; Kaminski and Jaupart, 1998). We therefore use a pseudogas approximation for the eruptive fluid to approximate a rhyolitic ash–gas composite mixture with 4 wt.% aqueous fluid. The eruptive fluid is specified as an ideal gas defined by its gas constant ($R_{fluid} = 18.46$ J kg^{-1} K^{-1}) and isentropic expansion coefficient ($\Gamma = 1.02$) based on its composition (Rudinger, 1980). We set the eruptive fluid velocity at the vent to be sonic for the pseudogas (150 m s^{-1} for both simulations) and set the temperature to 1200 K. Note that these inflow conditions are simplified steady-state conditions that do not consider the compositional, temporal, or spatial complexities resulting from conduit dynamics.

Simulations were performed using a modified version of CFDLib, a group of codes developed by the Theoretical Fluid Dynamics group at Los Alamos National Laboratory. CFDLib uses a cell-centered finite volume method and employs a modi-

Fig. 2. Snapshots of overpressured jets simulated with different resolutions. The 2 m cell size used for this study (a) was necessary to resolve the annular velocity profile in the overpressured case. A test case using 5 m grid cells (b) does not capture the Mach disk or the annular profile and behaves similarly to the pressure-balanced case. These snapshots are from the same time in both simulations.

fied version of the Godunov method to solve for high-speed compressible flows, including shocks (Kashiwa and Vander-Heyden, 2000). This robust numerical method is a key reason that CFDLib was chosen for this study since the velocity profiles examined in this paper are a direct consequence of the shape, size and strength of these shocks.

Ogden et al. (2008) show that a sonic volcanic jet issuing from an overpressured (OP) vent rapidly expands to a plume radius (r_{plume})

$$r_{plume\_OP} = r_{vent\_OP} K^{1/2} \qquad (1)$$

where r_{vent} is the vent radius and K the ratio of the vent pressure (P_{vent}) to the atmospheric pressure at the vent exit (P_{atm}). At the base of the plume, this rapid increase in plume radius in overpressured jets is due only to the rapid expansion and decrease in pressure. This expansion takes place up to a Mach disk, which exists at a height equal to about $1.7 r_{vent} K^{1/2}$ (Ogden et al., 2008). We set up two simulations of the same mass flow at the vent (M, kg s^{-1}) and the same plume radius after expansion, but with one jet issuing at atmospheric pressure and one at a pressure greater than atmospheric as shown with the following relationships. The mass flow at the vent is calculated by

$$M = \rho_{vent} \pi r_{vent}^2 v_{vent} \qquad (2)$$

where ρ_{vent} and v_{vent} are the density and vertical velocity at the vent. Using the ideal gas law and the fact that the fluid is erupting at atmospheric pressure, for the pressure-balanced (PB) case,

$$\rho_{vent\_PB} = \frac{P_{atm}}{R_{fluid} T_{vent}} \qquad (3)$$

For the overpressured case, however, the fluid erupts at a pressure equal to the atmospheric pressure at the vent times the overpressure ratio, giving

$$\rho_{vent\_OP} = \frac{K P_{atm}}{R_{fluid} T_{vent}} \qquad (4)$$

Combining Eqs. (3) and (4), the density of an overpressured case at the vent can be expressed as

$$\rho_{vent\_OP} = K \rho_{vent\_PB} \qquad (5)$$

since R_{gas}, T_{vent}, and P_{atm} are the same in both cases. Combining Eqs. (2) and (5), the mass flow at the vent for the both cases can be expressed as

$$M_{OP} = K \rho_{vent\_PB} \pi r_{vent\_OP}^2 v_{vent} \qquad (6a)$$

and

$$M_{PB} = \rho_{vent\_PB} \pi r_{vent\_PB}^2 v_{vent} \qquad (6b)$$

We choose two cases, one overpressured and one pressure-balanced, with different vent radii but the same composition, mass flow, temperature and velocity at the vent. Setting equal 6a
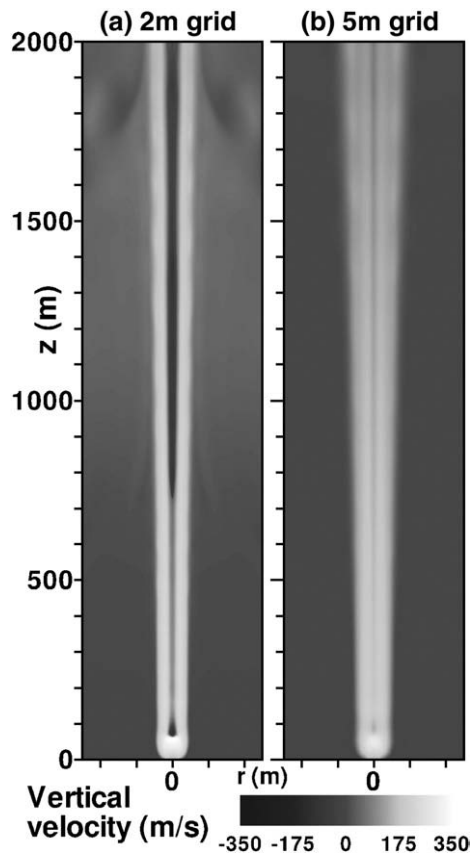
and 6b, we find that the relationship between these vent radii is expressed by

$$r_{\text{vent\_PB}}^2 = K r_{\text{vent\_OP}}^2 \qquad (7)$$

Combining Eqs. (1) and (7), we find that for these two jets with the same mass flow at the vent ($M = 3.5 \times 10^6$ kg s^{-1}), the vent radius of the pressure-balanced jet is equal to the plume radius of the overpressured jet after expansion.

We specify two simulations with moderate vent radii based on these relationships. The pressure-balanced case has a vent radius of 40 m. The overpressured case has a vent radius of 20 m and exits at a pressure that is 4 times atmospheric pressure. We have conservatively chosen this low value of vent overpressure (Woods and Bower, 1995) in order to minimize the effects of the strong turbulence that develops at higher pressures (Ogden et al., 2008). Both of these jets have the same vent mass flow, and, after expansion of the overpressured jet, both have a plume radius of about 40 m (Fig. 1). Both have the same surface area available for entrainment since both simulations have the same plume radius after decompression. The convective heat flow (Q, J s^{-1}) at the vent is

$$Q = M C_p (T_{\text{vent}} - T_{\text{atm}}) \qquad (8)$$

where C_p is the heat capacity of the fluid and T_{vent} and T_{atm} are the temperature of the fluid at the vent and of the surrounding atmosphere, respectively. These simulations therefore have the same heat flow at the vent ($Q = 2.8 \times 10^{12}$ J s^{-1}) since M, C_p, T_{vent}, and T_{atm} are the same for both simulations.

We have designed two simulated plumes with identical surface area available for air entrainment and vent heat flow using these relationships. These simulations compare only the effects of the different velocity profiles (resulting from the vent pressure condition) on the development and dynamics of a buoyant eruption column. They are not meant to fully capture the dynamics of any particular volcanic plume. Rather they are well-constrained numerical experiments that allow a simple first-order test of the effects of vent overpressure on a hot volcanic-scale plume.

3. Results

3.1. General flow structure

Both simulations develop buoyant plumes and well-defined gas-thrust and buoyant regions. The flow structure for the pressure-balanced case behaves as predicted by 1D theory (see Section 4). Fig. 3a shows a snapshot of the total density (air and eruptive fluid combined) for the pressure-balanced case. The gas-thrust region is clearly distinguished by the narrow region of high density relative to the surroundings at the base of the simulated column. The decrease in vertical velocity with height in this region can be seen in Fig. 4a. This region maintains a roughly steady height of about 1600 m. Turbulent eddies along the sides of the gas-thrust region entrain air into the plume (Fig. 5a), changing the plume above into a region that has a lower density (lighter colors) than the surrounding air (Fig. 3a). This buoyant region rapidly expands, turbulent eddies continue to entrain air and
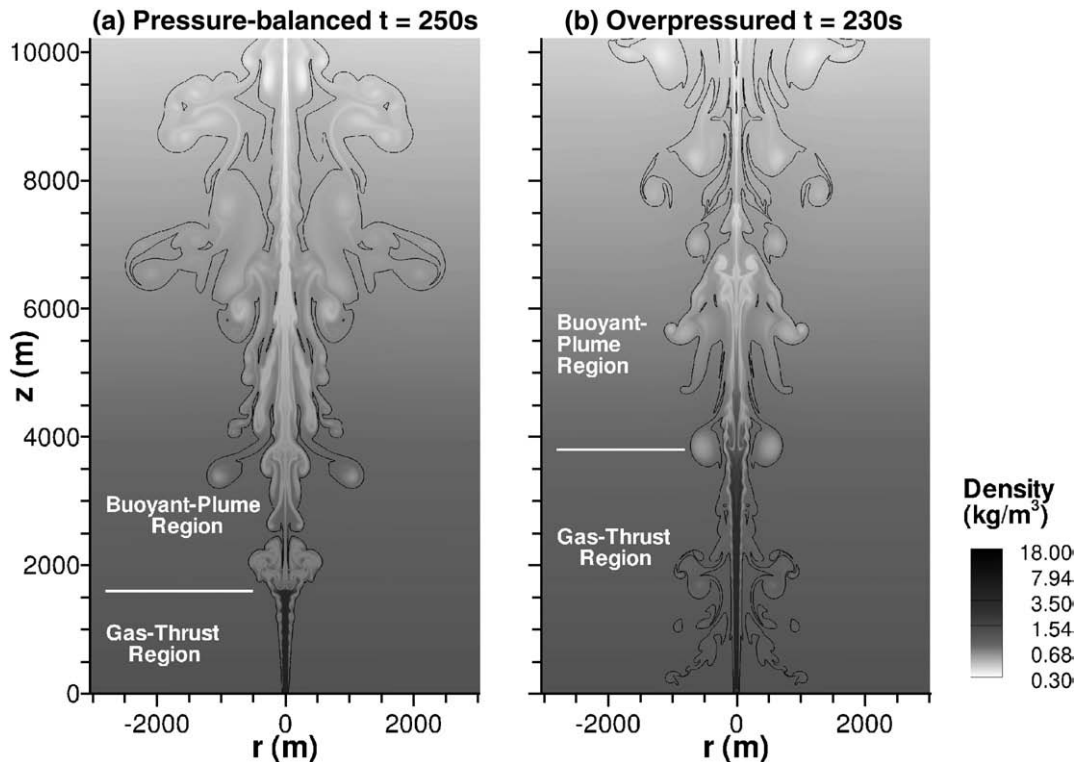

Fig. 3. Snapshots of density of the air and eruptive fluid combined. (a) Simulation with vent pressure equal to atmospheric pressure. (b) Simulation with vent pressure four times larger than atmospheric pressure. The solid line indicates the approximate visual boundary of the plume.
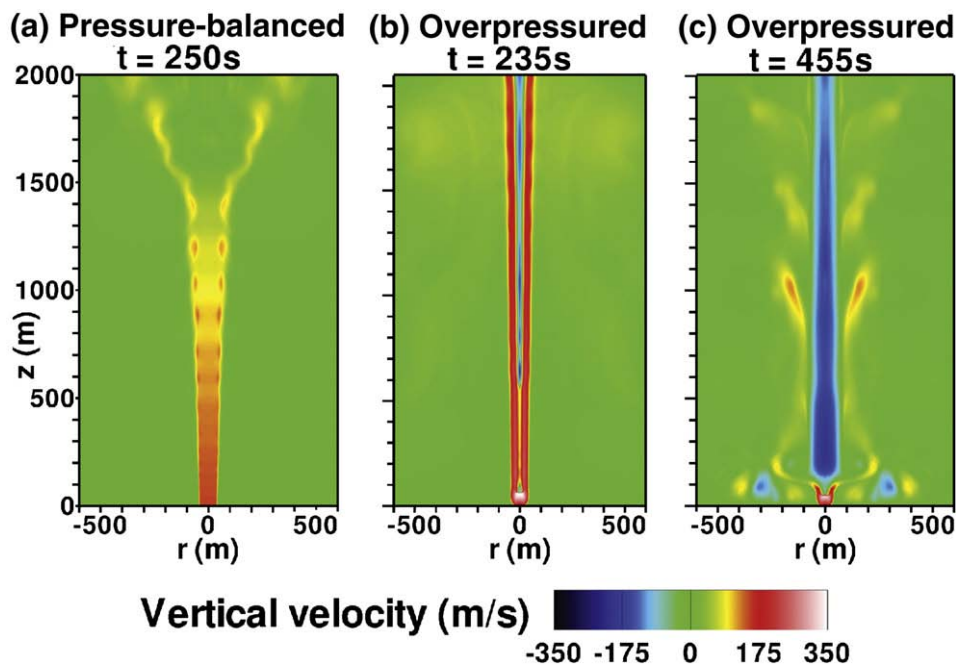
Author's personal copy

Fig. 4. Vertical velocity snapshots. (a) Simulation with vent pressure equal to atmospheric pressure. (b and c) Simulation with vent pressure four times larger than atmospheric pressure.

increase buoyancy, and the fluid accelerates until the fluid–air mixture passes out of the top boundary. Fig. 4a shows the increase in vertical velocity along the edges of the plume above the gas-thrust region as buoyant forces begin to take effect.

The overpressured case has a much more complicated and time-dependent flow structure than the pressure-balanced case. The flow undergoes rapid acceleration and expansion, forming an annular vertical velocity profile above a Mach disk at a height of about 60 m ($1.7r_{vent}K^{1/2}$) (Fig. 4b) as described in Ogden et al. (2008). This annular structure persists throughout the gas-thrust region up to about 3800 m (Fig. 3b), much higher than the gas-thrust region of the pressured balanced simulation. The overpressured plume transitions to a buoyancy driven plume at this higher point.
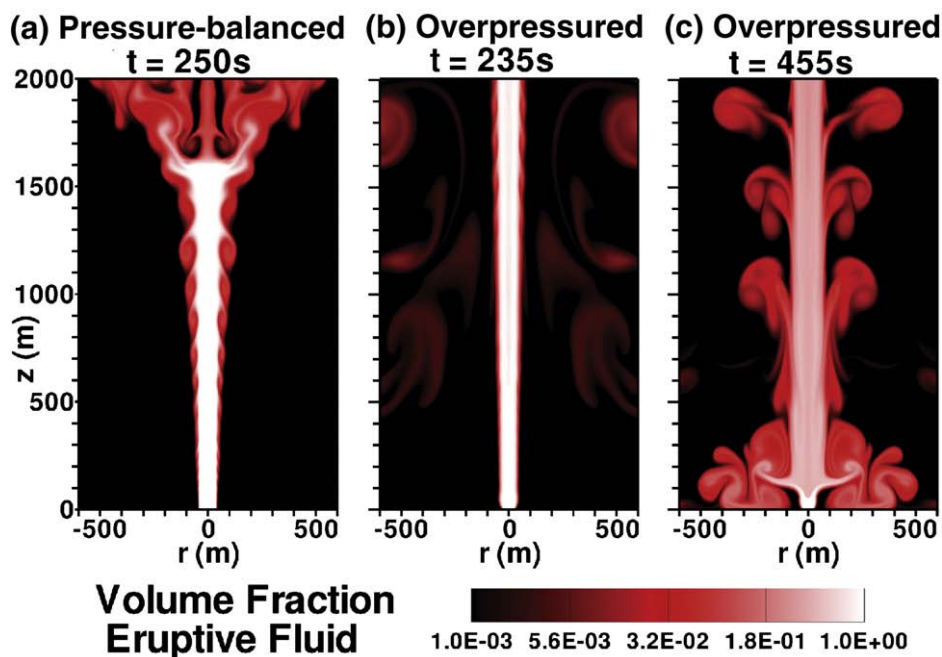

Fig. 5. Snapshots of volume fraction of eruptive fluid. (a) Simulation with vent pressure equal to atmospheric pressure. (b and c) Simulation with vent pressure four times larger than atmospheric pressure.

3.2. Oscillating collapse of the overpressured plume

The rapid expansion and formation of an annular velocity profile in the overpressured case also leads to an oscillating collapse of the plume. The overpressured plume begins with the majority of the fluid in the gas-thrust region moving rapidly upward. As the fast-moving annulus continues to move upward, the heavy fluid along the plume centerline decelerates, stops at about 3800 m and begins falling. The falling fluid spreads laterally when it reaches the Mach disk, crossing and disrupting the rising flow in the annulus. This fluid then "splashes" outward (Figs. 4c and 5c) just above the Mach disk and reaches the ground. The disruption of flow in the annulus destroys its upward inertia above the Mach disk (60 m). The plume then quickly recovers and inertially driven fluid once again reaches 3800 m and the process begins again. These collapses occur regularly about every 160 s in this simulation. If one defines the gas-thrust region as the region in which upward inertia dominates the flow field, then the height of the gas-thrust region oscillates between the Mach disk height (60 m) and about 3800 m due to these periodic column collapses. Fig. 3b shows a snapshot of the overpressured plume with the gas-thrust region at its peak height. The falling core fluid has had time to mix slightly with the surrounding air while near its highest point of accent and, although still not buoyant relative to the external atmosphere, is slightly more dilute than the fluid it falls passed in the annulus.

The reason this collapse occurs only in the overpressured case is likely due to the effects of the annular velocity profile, which is the main structural difference between the collapsing overpressured and non-collapsing pressure-balanced plumes. The heavy eruptive fluid is propelled upward by the inertia contained in the fast-moving fluid at the vent in both simulations. The eruptive fluid in the pressure-balanced case has enough inertia distributed throughout the plume to sustain the upward motion until enough mixing has occurred for the plume to become buoyant. The overpressured plume, however, is dominated by the annular velocity profile, which affects the stability of the gas-thrust region in two main ways. First, this velocity profile focuses the bulk of the upward momentum to the perimeter of the jet. The smaller upward inertia in the core of the plume is insufficient to counter the downward acceleration due to gravity. Second, the fast-moving annulus surrounding the slowly-moving core inhibits entrained air from reaching the core, precluding expansion and buoyancy production in the jet interior, as well as preventing eddies from crossing through the plume. Therefore, the gas-thrust region feeding the buoyant plume periodically collapses because the Mach disk forms a dense, slowly-rising core shielded from the outside entrained air even though the source conditions at the vent remain constant.

The downward moving fluid in the core also affects the entrainment dynamics within the gas-thrust region of the overpressured jet. More turbulent eddies form in this region while the core of the jet is moving downward due to the large shear between the upward flow in the annulus and the downward flow in the core. The collapsing fluid also pushes the plume wider during the downward phase of the oscillation, resulting in a disperse plume after each collapse (Figs. 4c and 5c). The plume radius in the gas-thrust region decreases to its original size (Figs. 4b and 5b) when the upward phase begins again.

3.3. Plume velocities through time

Comparing the vertical velocity within these plumes as a function of time at different radii and heights illustrates how these two simulations differ. Fig. 6 shows the vertical velocity at
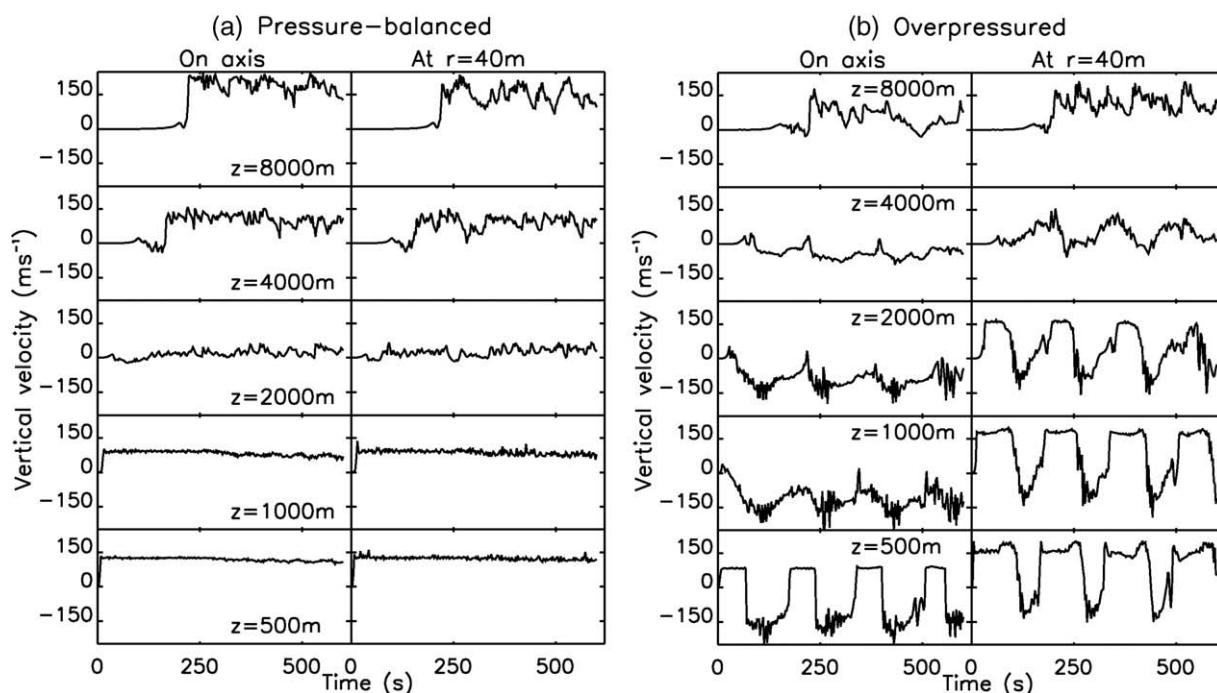

Fig. 6. Vertical velocity over time at 10 different locations. (a) Simulation with vent pressure equal to atmospheric pressure. (b) Simulation with vent pressure four times larger than atmospheric pressure.

five different heights along the jet centerline and at a radius of 40 m from the jet centerline for both simulations. This distal location was chosen because it is the predicted location of the approximate edge of the plume for both jets before air entrainment (Section 2).

The vertical velocity on the axis and at $r=40$ m shows roughly the same profile in the pressure-balanced case (Fig. 6a). The vertical velocity rapidly increases when the eruptive fluid arrives and then remains constant throughout the eruption within the gas-thrust region ($z=500$ m and 1000 m). The magnitude of this velocity decreases as the fluid moves from 500 to 100 m and loses momentum due to gravity. At 2000 m, just above the transition from the gas-thrust to the buoyant region, the vertical velocity of the fluid is on average about zero at the jet axis and slightly higher at $r=40$ m. More air has entrained and expanded along the edges of the jet, making it slightly more buoyant there than in the center. The column is dominated by buoyancy forces and accelerates with height as more air is entrained and expanded above 2000 m. The flow here becomes more time-dependent relative to the gas-thrust region, reflecting the large turbulent eddies that dominate the flow field in the buoyant region. However, the vertical velocity profile is still dominated by fast, upward moving fluid.

The overpressured case has very different vertical velocity profiles than the pressure-balanced case and is dominated by the oscillating collapse of the plume (Fig. 6b). The core of the jet in the gas-thrust region above 500 m is moving downward for the bulk of the simulation. In the buoyant region at 8000 m, enough air has been entrained into the core to maintain a buoyant rise. At 500 m, the fluid is still close enough to the vent that it is not yet completely decelerated by gravity. However, the downward moving fluid above periodically destroys this upward momentum, forcing all of the fluid along the centerline to move downwards. When this downward moving core is forced out laterally (e.g. Fig. 5c), the slightly delayed disruption of the fast-moving annulus is clearly seen (Fig. 6b). The vertical velocity in the annulus of the plume oscillates sharply and regularly between fast upflows and somewhat slower downflows. The effects of this highly periodic disruption are seen in the vertical velocity profiles throughout the height of the column and result in smaller and more time-dependent core velocities in the buoyant region (8000 m).

4. Discussion

4.1. Vent conditions as controlling parameters

Many 1D models use vent heat flow or mass flow as the important controlling parameter of plume dynamics (e.g. Woods, 1988). However, the two simulations presented here suggest that two plumes with the same vent heat and mass flows can result in very different plumes with different associated hazards. At a minimum, the overpressured simulation produces a gas-thrust region that periodically reaches a much higher altitude than the pressure-balanced simulation. We cannot compare total column heights since our simulation grid only extends to 10 km. A more complete study is necessary to

quantify the relationship between overpressure and the height of the gas-thrust region and the total plume height. To first order, our results suggest that even low overpressure ratios can markedly increase the height of the gas-thrust region and may have an effect on column stability.

4.2. Implications of an oscillating collapsing column with a steady source condition

Traditionally, transition from a buoyant to collapsing plume has been attributed to a change in source condition, e.g. a change in vent radius (Walker, 1981; Woods, 1988) or magma composition (e.g. Neri et al., 1998). Our simulations show that overpressured volcanic plumes may undergo this transition repeatedly without any change in source condition. These "transitional" columns, that are neither strictly buoyant nor collapsing, are also seen in the simulations of Neri et al. (2002) for both overpressured and pressure-balanced jets. In their simulations, whether the plume is buoyant, transitional, or collapsing is based on both overpressure and vent heat flow. The simulations of Neri et al. (2002) differ from those in this paper in a number of ways including a specification of a multiphase eruptive fluid and consideration of much larger overpressure and vent radii. It is significant that our simulations also reproduce this effect with a much simpler pseudogas eruptive fluid and for a much smaller plume. The simulations of this paper and Neri et al. (2002) along with field studies showing the existence of intraplinian pyroclastic flow deposits (e.g. Wright, 1981; Wilson and Hildreth, 1997) suggest that transitional columns may be a more common type of eruption plume than previously recognized. Further field studies and review of the literature may result in the identification of more of these deposits.

4.3. Comparison with laboratory experiments and 1D models

Kieffer and Sturtevant (1984) performed a series of laboratory experiments of overpressured volcanic jets using heavy gases as analogs for volcanic fluids. That study and numerous other laboratory studies of overpressured jets (e.g. Ladenburg et al., 1949; Lewis and Carlson, 1964; Antsupov, 1974) clearly show the development of the Mach disk, similar to this study. The flow field downstream of the Mach stem in laboratory experiments is very different from that of the volcanic-scale simulations of this study and Ogden et al. (2008). Laboratory experiments show rapid mixing of the fast-moving shear layer with the slow jet core and repeated, well-formed Mach disks and shock waves. Simulations with CFDLib of laboratory experiments reproduce these dynamics and the scaling of the Mach disk with height (Ogden et al., 2005; Ogden et al., 2008). Unlike the laboratory-scale experiments and simulations, the volcanic-scale simulations of this paper and Ogden et al. (2008) show a single Mach stem and a well-developed fast-moving annulus that maintains its profile for several kilometers into the plume.

The difference in dynamics downstream of the Mach disk between large- and laboratory-scale jets has also been shown in

other studies (Norman et al., 1982). This difference in flow dynamics between large and small scales is due to the non-linear relationships between various aspects of compressible flow, making the scaling of small-scale laboratory jet structures to those the size of volcanic eruptions very uncertain. A full discussion of these issues is beyond the scope of this paper, but we include one here for illustration. The formation of a second Mach disk is dependent upon the reflection of expansion waves off of the jet boundary. These reflected waves coalesce to form the Mach disk. The reflection is disturbed above the Mach disk if the jet boundary is too turbulent, precluding the development of a second Mach disk. Consider now the turbulence production along the jet boundary leading up to the height at which a second Mach disk would form. The vertical length scale (L) of this shear layer is roughly equal to the height of the first Mach disk. For a vent pressure of four times atmospheric, this is about 1 cm for the laboratory scale and 100 m for a small volcanic scale. The velocity scale (U) for both the laboratory and volcanic-scale jets with this overpressure is about 300 m/s. A good measure of turbulence is the Reynolds number, $Re = ULv^{-1}$, where v is the viscous diffusivity of the fluid. The Reynolds number of the volcanic-scale jet is four orders of magnitude larger than the laboratory-scale jet assuming these jets have the same viscosity. This increase in turbulence along the side of the jet is likely disrupting the reflection of expansion waves and the formation of a second Mach disk. This describes only one of a number of the effects of length scale leading to dynamics that prohibit the formation of more than one Mach disk. The key point is that the fluid velocities are independent of vent radius but the dimensions of the shock wave and lower portion of the jet are not.

The increase in turbulence with scale seems to suggest that the volcanic-scale jets should be more well mixed downstream of the Mach disk than the laboratory-scale jets, but this is not the case. This mixing occurs in radius as fluid mixes from the annulus to the core of the jet. This distance is much larger in the volcanic-scale jets resulting in less mixing across the centerline relative to the laboratory-scale jets. Gravity also becomes important after the first Mach disk. The interior of the jet is effectively stripped of its vertical momentum by the first Mach disk, and the density in this region is much higher than that of the surrounding air. Gravitational acceleration causes the initially more slowly-rising core region to start falling while the surrounding fast-moving annulus is rising since all the fluid is accelerated at the same rate (-9.8 m s^{-1}) until buoyancy becomes a factor. Laboratory experiments of overpressured jets should not be used to predict the fluid dynamics of an overpressured volcanic jet beyond the first Mach disk because these small-scale jets include repeating Mach disks and do not include buoyancy effects.

The overpressured simulation also shows both a larger plume radius after expansion and a smaller, cross-section averaged, vertical velocity than those predicted by the 1D models of Woods and Bower (1995). The analytical approximation of Woods and Bower neglects momentum loss along the sides of overpressured jets leading to an over-prediction of the velocity and under-prediction of the plume radius after expansion by about 25% at low overpressures and a factor of two at high

overpressures (Ogden et al., 2008). The 1D model of Woods and Bower also does not predict the oscillating plume of the overpressured jet since it does not take into consideration the radial velocity profile and unsteady behavior that causes this effect.

4.4. Caveats about our model approximations

The eruptive fluid in these simulations is specified as a pseudogas instead of a multiphase fluid. This approximation treats the ash–gas mixture as a heavy, high heat-capacity single fluid with an ideal gas equation of state and assumes that the ash particles remain evenly dispersed by mass fraction throughout the flow field and in thermal equilibrium with the gas. Kieffer and Sturtevant (1984) maintains that this is a good approximation for fine ash (<1 mm diameter) especially in the buoyant column where slip velocities between particles and gas are small. More dense loads of courser material in real eruptions may preclude the formation of a well-defined Mach stem and the resulting annular velocity profile.

The turbulent compressible dynamics of the supersonic annulus and resulting entrainment need to be modeled carefully. Communication within the fluid breaks down where fluid velocities approach the speed of sound, and turbulent entrainment no longer behaves as it does in subsonic shear layers, a very counterintuitive situation (Papamoschou and Roshko, 1988). In addition, as with any study of volcanic plumes, any complication that is known to affect the stability or energy
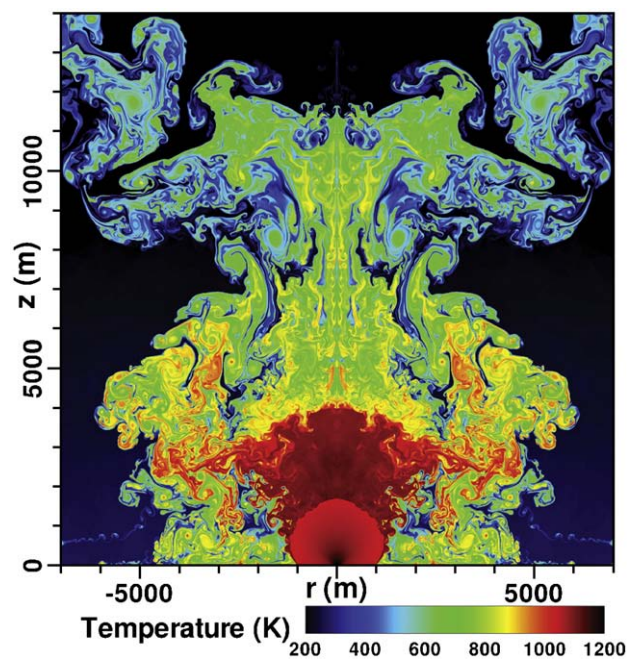

Fig. 7. Snapshot of large overpressured plume simulation. This snapshot of a simulation with a vent radius of 100 m and vent pressure of 100 times atmospheric pressure shows the much more complex, turbulent behavior of large eruptions. Despite the large amount of mixing in this simulation, the center of the plume remains negatively buoyant with respect to the surrounding air.

dynamics of an eruption column may influence the annular velocity profile of an overpressured jet, including wind shear, water condensation and unsteady source conditions. We have also chosen a very small overpressure to limit the amount of turbulence (and therefore complexity) of the flow field. Preliminary simulations of plumes with larger overpressures and vent radii show a much more chaotic flow field (Fig. 7) but still have fluid falling in the core of the jet.

The choice of using a 2D axisymmetric model enabled us to complete a number of high-resolution calculations, but it also introduced some limitations. It is possible that the oscillation seen in our overpressured case is the result of the symmetry condition and two-dimensionality. Turbulent mixing is a 3D process and can only be robustly simulated in 3D (Suzuki et al., 2005). We have also precluded any flow or mixing across the vertical axis of the jet by specifying axisymmetry. If the slow-moving core of the jet mixed more efficiently with the fast-moving annulus, the core might not collapse. It's possible that the symmetry condition and limitation to 2D is prohibiting mixing between the core and the annulus, resulting in a heavy, collapsing core. However, our simulation of a much larger eruption with a vent radius of 100 m and an overpressure of 100 times atmospheric (Fig. 7) still shows downflow along the jet centerline and maintains both collapsing and buoyant dynamics despite the large amounts of turbulent mixing. Both simulations are 2D, however, which cannot truly capture entrainment dynamics. Although these simulations suggest overpressured vents may lead to transitional columns, a series of fully 3D simulations is required to robustly capture entrainment dynamics and mixing across the centerline and fully quantify the effect of vent overpressure on plume dynamics.

5. Conclusions

We have shown that vent overpressure may have a significant effect on plume dynamics including that in the buoyant regime by comparing a 2D simulation of an over-pressured volcanic jet with that of a pressure-balanced volcanic jet. We specified these jets to have the same mass and heat flow at the vent, and, after initial expansion of the overpressured jet, they have the same plume radius. These simulations suggest the following conclusions, which need to be tested with 3D simulations:

1) In comparison to pressure-balanced jets with the same vent heat flow, vent overpressure increases the maximum altitude of the transition from the inertia-dominated to buoyancy-dominated regime of the associated eruption column.
2) The annular vertical velocity profile predicted by Ogden et al. (2008) for the jets in the absence of gravity appears to persist throughout the gas-thrust region of buoyant columns affecting air entrainment rates and mixing with the ambient air.
3) Some overpressured vents may result in oscillations between buoyant and collapsing columns without any changes of source condition and may explain the presence of intrapli-nian pyroclastic flow deposits.

Appendix A. Standard Earth atmosphere profile

The change in pressure, density, and temperature with height of the initial model atmosphere are calculated using a standard Earth atmosphere model. The exact profiles for temperature (T), pressure (P), and density (ρ) as a function of height (H) are as follows.

$$T = T_b + L(H - H_b) \tag{A1}$$

$$P = P_b \left(\frac{T}{T_b}\right)^{-\frac{g_0 M}{RL}} \tag{A2}$$

$$\rho = \frac{MP}{RT} \tag{A3}$$

M is the molecular weight of air, 28.96, and R is the universal gas constant. g_0 is the gravitational acceleration at sea level (9.81 m s^{-2}). For heights below 11 km, $H_b=0$ m, $L=-6.5$ K km^{-1}, $T_b=288.15$ K, $P_b=101\,325$ Pa.

References

Aloisi, M., D'Agostino, M., Dean, K.G., Mostaccio, A., Neri, G., 2002. Satellite analysis and PUFF simulation of the eruptive cloud generated by the Mount Etna paroxysm of 22 July 1998. J. Geophys. Res. 107. doi:10.1029/2001JB000630.

Antsupov, A.V., 1974. Properties of underexpanded and overexpanded supersonic gas jets. Soviet Phys. Tech. Phys. 19, 234–238.

Bonadonna, C., Connor, C.B., Houghton, B.F., Connor, L., Byrne, M., Laing, A., Hincks, T., 2005. Probabilistic modeling of tephra dispersion: hazard assessment of a multi-phase eruption at Tarawera, New Zealand. J. Geophys. Res. 110. doi:10.1029/2003JB002896.

Carazzo, G., Kaminski, E., Tait, S., 2006. The route to self-similarity in turbulent jets and plumes. J. Fluid Mech. 547, 137–148.

Carey, S., Sparks, R.S.J., 1986. Quantitative models of the fallout and dispersal of tephra from volcanic eruption columns. Bull. Volcanol. 48, 109–125.

Connor, C.B., Hill, B.E., Winfrey, B., Franklin, N.M., LaFemina, P.C., 2001. Estimation of volcanic hazards from tephra fallout. Nat. Hazards Rev. 2, 33–42.

Hurst, A.W., Turner, R., 1999. Performance of the program ASHFALL for forecasting ashfall during the 1995 and 1996 eruptions of Ruapehu volcano. New Zealand J. Geol. Geophys. 42, 615–622.

Ishimine, Y., 2006. Sensitivity of the dynamics of volcanic eruption columns to their shape. Bull. Volcanol. 68, 516–537.

Kaminski, E., Jaupart, C., 1998. The size distribution of pyroclasts and the fragmentation sequence in explosive volcanic eruptions. J. Geophys. Res. 103, 29759–29779.

Kaminski, E., Tait, S., Carazzo, G., 2005. Turbulent entrainment in jets with arbitrary buoyancy. J. Fluid Mech. 526, 361–376.

Kashiwa, B.A., VanderHeyden, W.B., 2000. Toward a general theory for multiphase turbulence Part I: Development and gauging of the model

equations. Los Alamos National 698 Laboratory Report. Los Alamos National Laboratory, Los Alamos, NM, p. 88.

Kieffer, S.W., 1981. Blast dynamics at Mount St. Helens on 18 May 1980. Nature 291, 568–570.

Kieffer, S.W., Sturtevant, B., 1984. Laboratory studies of volcanic jets. J. Geophys. Res. 89, 8253–8268.

Koyaguchi, T., Ohno, M., 2001a. Reconstruction of eruption column dynamics on the basis of grain-size of tephra-fall deposits: part 1. Methods. J. Geophys. Res. 106, 6499–6512.

Koyaguchi, T., Ohno, M., 2001b. Reconstruction of eruption column dynamics on the basis of grain-size of tephra-fall deposits: part 2. Application to Pinatubo. J. Geophys. Res. 106, 6513–6533.

Ladenburg, R., Van Voorhis, C.C., Winckler, J., 1949. Interferometric studies of faster than sound phenomena. Part II. Analysis of supersonic air jets. Phys. Rev. 76, 662–677.

Lewis, C.H.J.R., Carlson, D.J., 1964. Normal shock location in underexpanded gas and gas-particle jets. AIAA Journal 2, 776–777.

Macedonio, G., Pareschi, M.T., Santacroce, R., 1990. Renewal of explosive activity at Vesuvius: models for the expected tephra fallout. J. Volcanol. Geotherm. Res. 40, 327–432.

Morton, B.R., Taylor, G., Turner, J.S., 1956. Turbulent gravitational convection from maintained and instantaneous sources. Proc. R. Soc. Lond., Series A, Math. Phys. Sci. 234, 1–23.

Neri, A., Papale, P., Macedonio, G., 1998. The role of magma composition and water content in explosive eruptions: 2. Pyroclastic dispersion dynamics. J. Volcanol. Geotherm. Res. 87, 95–115.

Neri, A., Di Muro, A., Rosi, M., 2002. Mass partition during collapsing and transitional columns by using numerical simulations. J. Volcanol. Geotherm. Res. 115, 1–18.

Neri, A., Ongaro, T.E., Menconi, G., Vitturi, M.D., Cavazzoni, C., Erbacci, G., Baxter, P.J., 2007. 4D simulation of explosive eruption dynamics at Vesuvius. Geophys. Res. Lett. 34. doi:10.1029/2006GL028597.

Norman, M.L., Smarr, L., Winkler, K.H.A., Smith, M.D., 1982. Structure and dynamics of supersonic jets. Astron. Astrophys. 113, 285–302.

Ogden, D.E., Wohletz, K.H., Glatzmaier, G.A., Peterson, A.H., 2005. Preliminary benchmarking of numerical simulations of the supersonic behavior of Plinian eruptions. Eos Trans. AGU 86 (52) Fall Meet. Suppl., Abstract V34B-07.

Ogden, D.E., Wohletz, K.H., Glatzmaier, G.A., Brodsky, E.E., 2008. Numerical simulations of volcanic jets: Importance of vent overpressure. J. Geophys. Res. 113 B02204, doi:10.1029/2007JB005133.

Papale, P., Neri, A., Macedonio, G., 1998. The role of magma composition and water content in explosive eruptions — 1. Conduit ascent dynamics. J. Volcanol. Geotherm. Res. 87, 75–93.

Papamoschou, D., Roshko, A., 1988. The compressible turbulent shear layer: an experimental study. J. Fluid Mech. 197, 453–477.

Rudinger, G., 1980. Fundamentals of Gas-particle Flow. Elsevier Sci., New York.

Searcy, C., Dean, K., Stringer, W., 1998. PUFF: a high-resolution volcanic ash tracking model. J. Volcan. Geotherm. Res. 80, 1–16.

Sparks, R.S.J., Wilson, L., 1976. A model for the formation of ignimbrite by gravitational column collapse. Jour. Geol. Soc. London 132, 441–451.

Sparks, R.S.J., Bursik, M.I., Carey, S.N., Gilbert, J.S., Glaze, H., Sigurdsson, H., Woods, A.W., 1997. Volcanic Plumes. Wiley, New York.

Suzuki, Y.J., Koyaguchi, T., Ogawa, M., Hachisu, I., 2005. A numerical study of turbulent mixing in eruption clouds using a three-dimensional fluid dynamics model. J. Geophys. Res. 110. doi:10.1029/2004JB003460.

Valentine, G.A., Wohletz, K.H., 1989. Numerical-models of Plinian eruption columns and pyroclastic flows. J. Geophys. Res. 94, 1867–1887.

Walker, G.P.L., 1981. Plinian eruptions and their products. Bull. Volcanol. 44, 223–240.

Walker, G.P.L., Wilson, L., Bowell, E.L.G., 1971. Explosive volcanic eruptions I: the rate of fall of pyroclasts. Geophys. J. R. Astron. Soc. 22, 377–383.

Wilson, C.J.N., Hildreth, W.H., 1997. The Bishop Tuff: new insights from eruptive stratigraphy. J. Geol. 105, 407–439.

Wilson, C.J.N., Hildreth, W., 1998. Hybrid fall deposits in the Bishop Tuff, California: a novel pyroclastic depositional mechanism. Geol. 26, 7–10.

Wilson, L., Sparks, R.S.J., Huang, T.C., Watkins, N.D., 1978. The control of volcanic column heights by eruption energetics and dynamics. J. Geophys. Res. 83, 1829–1836.

Woods, A.W., 1988. The fluid dynamics and thermodynamics of eruption columns. Bull. Volcanol. 50, 169–193.

Woods, A.W., Bower, S.M., 1995. The decompression of volcanic jets in a crater during explosive volcanic eruptions. Earth Planet. Sci. Lett. 131, 189–780.

Wright, J.V., 1981. The Rio Caliente ignimbrite: analysis of a compound intraplinian ignimbrite from a major late Quaternary Mexican eruption. Bull. Volcanol. 44, 189–212.